64-PIXEL SOLID STATE CMOS COMPATIBLE ULTRASONIC FINGERPRINT READER

Justin C. Kuo[1], Jason T. Hoople[1], Mamdouh Abdelmejeed[1], Mohamed Abdel-moneum[2] and Amit Lal[1]
[1]School of Electrical and Computer Engineering, Cornell University, Ithaca, NY, USA
[2]Intel Corporation, USA

ABSTRACT

We report on a 1D linear array of GHz ultrasonic transducers as an ultrasonic impedance imager for fingerprint sensing. This device is based on an all solid state aluminum nitride (AlN) transducer array that eliminates the need for released membranes. Compared to lower frequency (10-50 MHz) ultrasonic sensors, our device uses GHz ultrasonic pulses, generated by driving AlN pixel transducers at resonance with 1.3 GHz RF pulses at a CMOS compatible voltage of 2V. In addition to faster acquisition speed, GHz ultrasonic imaging enables much higher resolution owing to the smaller wavelength by phase driving several pixels. From noise levels of signals and point measurements, we estimate that the ultimate single point resolution possible for the sensor is 15-20 um or ~1700 dpi.

INTRODUCTION

As electronics are increasingly integrated into all aspects of our lives, the use of biometric sensors, such as fingerprint readers, is becoming critical to ensuring the safety of personal data. Commercial fingerprint sensors are available in a variety of imaging modalities such as capacitive sensing, which is deployed in IPhones, and emerging ultrasound imagers from key players in the industry.

Of particular interest is the ultrasonic fingerprint sensor, which is capable of imaging the elastic properties of the surface placed on the sensor surface, thereby providing additional protection against spoofing. Recent ultrasonic fingerprint readers have been motivated by PMUTs [1] and CMUTs [2] – however, both involve released membrane actuators that have to be packaged appropriately to prevent damage to the membrane. Membrane based actuator arrays also have to compensate for cross-coupling to neighboring pixels. Alternative solutions that utilize PZT pillars minimize damage and cross-coupling issues, but require a non-lithography based manufacturing process and are limited to lower frequencies of a few MHz[3]. An all solid state device that enables the smallest form factor, lowest power that can benefit from low voltage-high speed modern CMOS and effectively couple the energy through glass surfaces to human tissue, is needed.

This work builds upon previous work on on-chip phased array ultrasonic communication links, sonic memory and single pixel elastic impedance imaging [4] [5] [6]. In [4], it was demonstrated that a single transducer can be used to image materials applied on the backside of a silicon die and thereby be used for fingerprint imaging.

In this work, we utilize a linear array of 64 such transducers in conjunction with a multiplexed transmit-receive circuit to image a fingerprint phantom at high resolution, as well as demonstrate the possibility of sub-pixel resolution through diffraction. Because a linear array is used, it is possible to image the entirety of a fingerprint simply by scanning the finger in a single direction.

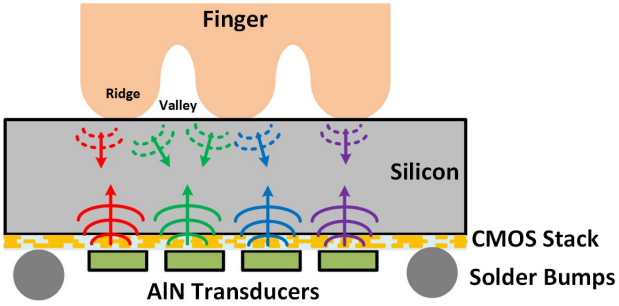

Figure 1: GHz ultrasonic fingerprint sensing. Diffraction effects enable each individual transducer to pick up signals from multiple features. As the acoustic wavelength in silicon is on the order of the thickness of the CMOS stack, acoustic waves are able to pass into low-loss bulk silicon with minimal loss

As shown in Fig. 1, a GHz ultrasonic pulse is emitted from a transducer by exciting it with a RF voltage pulse. The ultrasound travels through the thickness of the silicon and reflects off the backside interface. The reflected wave travels back to the transducer and generates a voltage pulse. If there is no fingerprint ridge present on the backside of the silicon, the backside is a silicon-air interface. Due to the low acoustic impedance of air (400 Rayl), all of the energy reflects back into the silicon. If a fingerprint ridge is present, some of the acoustic energy is coupled into the finger, and the received signal is reduced. For a wave traveling from medium 1 to medium 2, the amount of energy reflected back into medium 1 at the interface is determined by the reflection coefficient Γ, as defined in (1).

$$\Gamma = (Z_2 - Z_1)/(Z_2 + Z_1) \quad (1)$$

The elastic impedance of skin is 1.76 MRayl [11] and the elastic impedance of silicon is 17.4 MRayl. Thus, the amount of energy reflected into the silicon, when the backside is loaded with a fingerprint ridge, is 0.82 times the amount that is reflected back when the backside is air loaded. As the acoustic reflection signal is only received after the signal travels through the thickness of the silicon, there is a delay T_{Delay} between the transmit pulse and the received acoustic pulse, as defined in (2).

$$T_{Delay} = 2L_{Si}/c_{Si} \quad (2)$$

For the nominal silicon thickness L_{Si} of 725 µm and velocity of bulk acoustic waves in silicon c_{Si} of 8400 m/s, there will be a delay of approximately 170 ns between the transmit and receive signals. Because the excitation voltage will be greater than the received voltage from the first acoustic reflection, this imposes the constraint that the excitation pulse should be shorter than the delay to prevent the transmit and receive signals from overlapping.

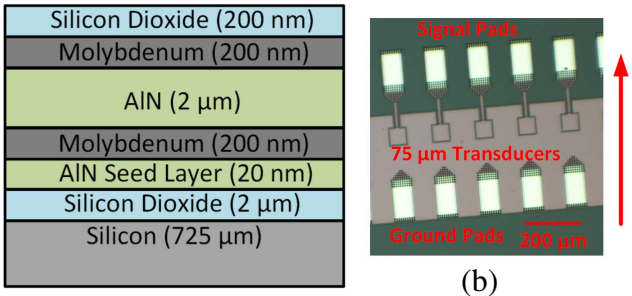

Figure 2: (A) Nominal thin film layer thicknesses used for device. (B) Transducers used in the linear array. Imaging is performed by swiping across the array in the direction indicated by the arrow.

Each element in the linear array is an AlN transducer fabricated on a double side polished silicon substrate with molybdenum top and bottom electrodes and silicon dioxide thin film layers above and below the transducer. The nominal layer thicknesses for these devices is shown in Fig. 2. The thickness of these layers can be designed for optimal response at a frequency of interest, as described in [7]. The layer configuration used for this work gives optimal response at 1.3 GHz – this requires AlN films between 2 µm to 3 µm thick – and was fabricated at the Institute of Microelectronics (A*STAR IME) in Singapore. While other materials such as PZT have higher piezoelectric coupling factors, AlN is compatible with CMOS processing [8] and thus for a CMOS integrated solution, AlN is the piezoelectric film of choice.

The electrical to acoustic conversion loss in piezoelectric transducers can be modeled using the KLM model, as in Fig. 3, which can be evaluated using transfer matrices [9]. Alternatively, circuit simulators can be used with a modified version of Mason's model [10]. FEM simulation of devices is performed using PZFlex.

The other main source of loss is from diffraction – viscoelastic loss in silicon is small due to the crystalline nature of the material. For isotropic media, the bulk pressure wave radiated by a rectangular transducer of width W and height H at a distance z in the far field can be described by (3) [9].

$$p(x,y,z) \approx \frac{j\omega\rho v}{2\pi R} e^{-jk\left(z+\frac{x^2+y^2}{2z}\right)} WH * sinc\left(\frac{Wx}{\lambda z}\right) sinc\left(\frac{Hy}{\lambda z}\right) \quad (3)$$

Where v is the velocity of the transducer, ω is the frequency of actuation, ρ is the density of the medium, and $R = \sqrt{x^2+y^2+z^2}$. Using (3), we can estimate that approximately half of the emitted pressure is lost due to diffraction for the design presented in this paper. Smaller transducers will exhibit greater diffraction losses than larger transducers, while making pixels larger to reduce diffraction leads to lower resolution.

The pulse-echo response as a function of frequency and its measurement setup is shown in Fig. 4. The output amplitude of the RF switch into a 50 Ω oscilloscope input at 1.3 GHz is 1.8 Vpp. When a transducer is connected between the RF switch output and oscilloscope input, the amplitude of the first acoustic signal is 38 mVpp, but the electrical excitation signal has also dropped to 280 mVpp due to electrical impedance mismatch. The ratio of these two signals is not the true frequency response of the

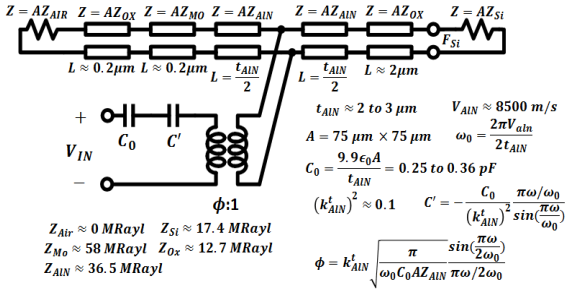

Figure 3: Transducer performance can be evaluated through the KLM model. Diffraction loss should be separately considered to obtain the complete transfer function.

transducer, due to the use of long wire bonds (7 to 8 mm) and the short, but finite length, connector and PCB trace length between the RF switch, the transducer, and the oscilloscope input. This ratio as plotted in Fig. 4 is approximately an order of magnitude greater than the transducer frequency response that is calculated using the KLM model.

EXPERIMENTAL METHODS

The circuit used to acquire data from the transducer array consists of three main portions – a transmit path, a receive path, and a cascade of RF switches – as seen in Fig. 5. The transmit path generates a 2 Vpp, 85 ns wide, 1.3 GHz RF pulse used for exciting the transducers – this is generated through the use of a VCO and a RF switch, the output of which is amplified. The receive path amplifies the receive signal with a cascade of 2 amplifiers (18 dB gain). The output from the amplifiers is then passed into an envelope detector, which converts the received acoustic signal to a baseband pulse. This pulse is digitized by an oscilloscope (Agilent DSO-X 91304A) and the received data is processed in MATLAB. Low pass filters are used to reduce high frequency noise from the transmit driver and can be eliminated with improved electronics design.

The AlN transducer array die is attached to the backside of a printed circuit board (PCB) and wire bonded to interface with onboard electronics through a cutout in the PCB. Each transducer in the linear array is connected to a

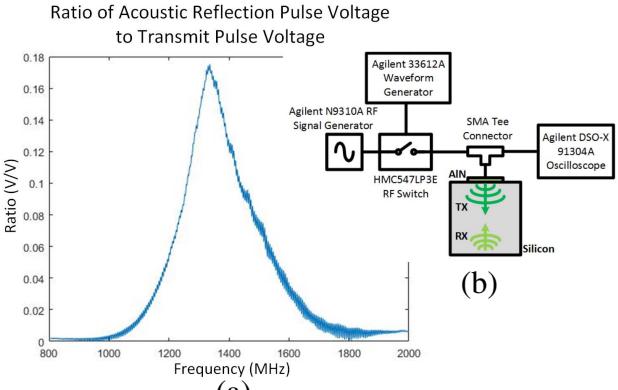

Figure 4: (A) Ratio of the amplitude of the first acoustic reflection signal to the amplitude of the transmit pulse for a 75 µm square transducer used in the linear array. (B) Measurement setup

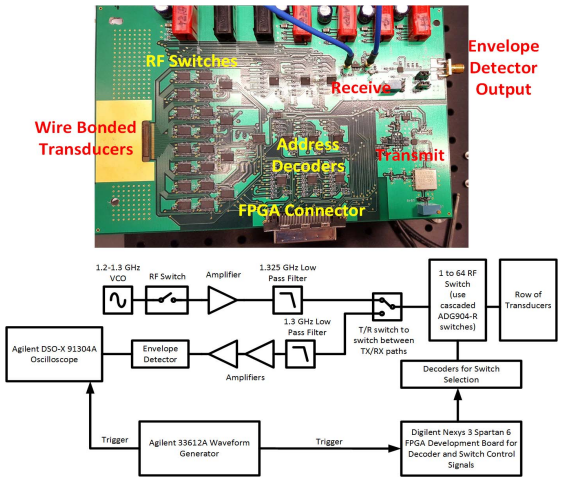

Figure 5: Block diagram of multiplexed transmit-receive circuit and PCB with wire bonded transducer

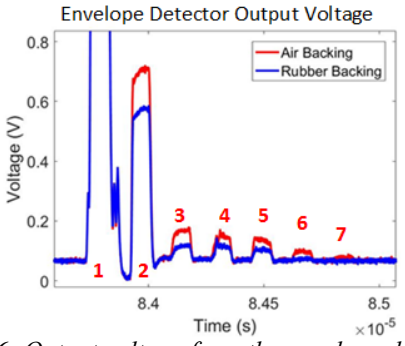

Figure 6: Output voltage from the envelope detector – upon loading by a rubber phantom, the acoustic reflection signal is reduced. Pulse 2 is the first acoustic signal, the primary signal of interest. Pulse 1 corresponds to electrical coupling and occurs at the same time as the transmit pulse. Pulses 3 to 7 are multiple acoustic reflections.

terminal of a RF switch (AD904-R). These RF switches are connected in cascade to form a 64 to 1 RF switch, which is used to route transmit and receive signals to and from each transducer.

A FPGA board (Digilent Nexys 3) is used to control the onboard RF switches for transducer pixel selection and to generate the RF switch control pulse for the transmit circuitry. The primary reason a FPGA is used is to switch between the transmit and receive signal fast enough so that the received acoustic signal can be sampled – as the transmit pulse is 85 ns long and the delay time for the first acoustic signal to travel through the silicon, reflect off the interface, and reach the transducer again is 170 ns, this leaves 85 ns to switch between the transmit and receive circuits.

A rubber phantom is used to evaluate the fingerprint imaging due to the ease of scanning a phantom across the array in precise spatial increments, thereby reducing the complexity of image formation. The acoustic impedances of various rubbers varies between 1 to 2 MRayl [12], which is similar to the impedance of human tissue. A silicon mold of a fingerprint is first created using laser micromachining (LPKF Protolaser U). Rubber is pressed into the mold at high temperature to create the phantom. A Newport UTM150CC.1 translation stage, in conjunction with a Newport ESP300 motion controller, is used to scan the phantom across the array.

RESULTS AND DISCUSSION

The rubber phantom is scanned across the array at a resolution of 50 µm. In Fig. 6, we see the attenuation of the signal upon loading with rubber. Assuming a 2 MRayl impedance for rubber, we expect a reflection coefficient of 0.89. The envelope detector output for an air backed signal is 0.7 V. The voltage drops by approximately 0.1V, which corresponds to the expected reflection coefficient.

The image obtained from scanning the fingerprint phantom across the array is shown in Fig. 7, obtained by plotting the voltage difference between the output voltage corresponding to the first acoustic reflection signal for air backing and for the current scan point. There are 3 dead pixels in the image due to wire bonding errors.

To demonstrate the possibility of subpixel resolution, we fabricated rubber tips that are approximately 90 µm in diameter at the tip and scanned the tips across the backside of the array, as shown in Fig. 8, at 1 µm resolution. As the tips are scanned across the array, the output voltage from a transducer pixel begins to drop when the tip is 100 µm from the center of the transducer. When the pixel is completely covered by the rubber tip, the signal reaches its minimum value. As the tip moves away from the transducer, the voltage increases until it reaches the air-backed value. The transducer is therefore sensitive to material is that is placed up to 100 µm from its center on the silicon backside, for a 200 µm wide region of sensitivity. The width of this region can be estimated from the full width half maximum (FWHM) of the center lobe of the transducer radiation, defined for a square transducer in far field by (4) [13].

$$FWHM = 1.206\lambda z/W \quad (4)$$

Where λ is the acoustic wavelength in the medium, z is the propagation distance, and W is the width of the transducer. For 1.3 GHz frequency and assuming isotropic propagation in silicon, the FWHM can be estimated to be 150 µm wide, which is slightly smaller than the observed distance.

The amount of time required to excite a transducer pixel and switch to the next pixel in the array is 1.89 µs. This is limited primarily by the setup time for the onboard decoders to set the correct RF switch address for the next pixel to be measured. The minimum possible time required to sample a pixel is T_{MIN}, as defined in (5), where T_{PULSE} is the excitation pulse width (85 ns) and T_{DELAY} is the acoustic delay time (170 ns) from (2).

$$T_{MIN} = 2T_{PULSE} + T_{DELAY} = 2T_{PULSE} + 2L_{Si}/c_{Si} \quad (5)$$

This expression assumes that the multiple reflections can be reduced with increased diffraction, absorbing layers, or with a matching layer to the finger. If subdermal features are of interest, the additional propagation time for those features need to be taken into account. For the current system, there is an additional acquisition time imposed by the transfer of data from oscilloscope to the PC. This can be eliminated with an integrated ADC and onboard data processing. Therefore, in an ideal system, the entire array can be sampled every $64 \times t_{MIN}$ seconds, or 22 µs for the devices in this work.

The sensitivity of the system is determined by the electrical noise on the output signal. The noise value of 20

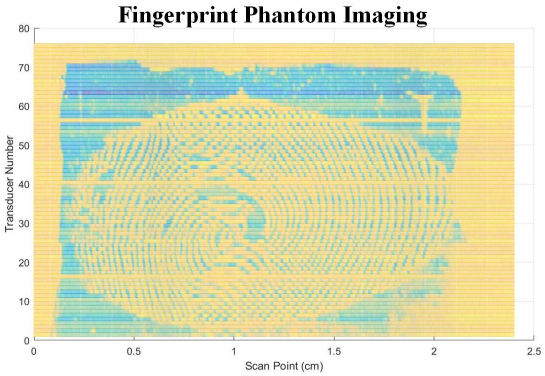

Figure 7: Image of fingerprint generated by scanning a fingerprint phantom along the array and plotting the voltage difference between loaded and unloaded conditions. Each transducer is spaced 200 µm apart in the array and the scan resolution is 50 µm. Because the phantom was offset, two scans were combined, hence the transducer number is greater than 64.

mV in Fig. 8 corresponds to a displacement of 15 to 20 µm – this is the minimum resolution resolvable for the system. The amount of displacement is dependent on the properties of the material to be imaged, as a material with an impedance closer to that of silicon would receive more acoustic energy from an incident pulse, and therefore the first acoustic reflection signal exhibits greater voltage change for the same drive conditions.

It can be noted that in Fig. 8 the background DC levels for the output voltage corresponding to the 4 transducers are different (0.62V for transducer 5 to 0.7V for transducer 4). As the traces connecting each transducer to a RF switch have different lengths and are connected to different RF switches in different regions of the PCB, the signal paths and parasitics for each channel are different and hence the off-state RF coupling (when the transmit switch is off) for each channel is different, and is resolved by the envelope detector as different background DC levels.

DISCUSSION AND CONCLUSIONS

While the measurements in this work were performed at a single frequency, it is possible to sweep excitation frequencies to increase differentiation between different materials, as shown in [4] for water, acetone, and isopropyl alcohol. Furthermore, we envision the use of phased array transducers to allow dynamic steering and focusing to improve imaging resolution.

An important topic for future investigation is whether absorption of high frequency ultrasound in tissue may be an issue for sub-dermal imaging applications. As discussed in [4], the attenuation should be small enough to allow for such purposes. Penetration depth can be increased by reducing frequencies to a few hundred MHz at the expense of resolution.

Another major complexity of our approach is the requirement for GHz electronics to process the data. At highly scaled CMOS technologies, this limitation is circumvented by both the speed and density of transistors. Integration of sensor arrays with CMOS circuits is a subject of ongoing work.

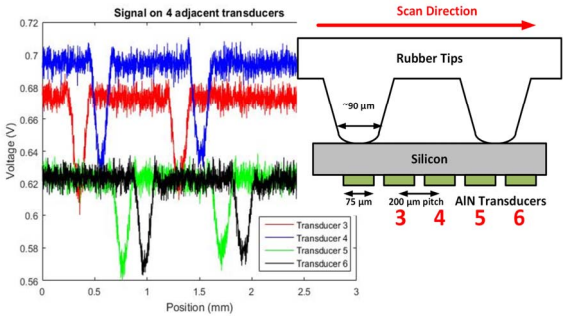

Figure 8: Signal on adjacent array elements when rubber tips are scanned along the array.

ACKNOWLEDGEMENTS

We would like to acknowledge the Cornell Nanoscale Facility (National Science Foundation Grant ECCS-1542081) for use of facilities and equipment. This work was also supported by the I-ARPA TIC program, and a grant from Intel Corporation.

REFERENCES

[1] Y. Lu, et al., "Ultrasonic fingerprint sensor using a piezoelectric micromachined ultrasonic transducer array integrated with complementary metal oxide semiconductor electronics", Appl. Phys. Lett., 106 (2015), 263503

[2] N. Lamberti, et al., "A high frequency cMUT probe for ultrasound imaging of fingerprints", Sensor Actuat. A-Phys., 172 (2011) pp. 561-569.

[3] R. Schmitt, et al., "Ultrasonic Imaging of Fingerprints using Acoustical Impediography", IEEE IUS 2012, pp. 1075-1085.

[4] J. Hoople, et al., "Chipscale GHz Ultrasonic Channels for Fingerprint Scanning", IEEE IUS 2015.

[5] J. Hoople, et al., "Chip-Scale Reconfigurable Phased-Array Sonic Communication", IEEE IUS 2014.

[6] J. Kuo, et al., "Towards a CMOS compatible delay line memory", IEEE IUS 2015.

[7] J. Hoople, et al., "Optimized Response of AlN Stack for Chipscale GHz Ultrasonics", IEEE IUS 2015.

[8] R. Olsson, et al., "Post-CMOS Compatible Aluminum Nitride MEMS Filters and Resonant Sensors", IEEE IFCS 2007.

[9] R. Cobbold, *Foundations of Biomedical Ultrasound*, Oxford University Press, 2007.

[10] W. Leach, "Controlled-Source Analogous Circuits and SPICE Models for Piezoelectric Transducers," IEEE Trans. Ultrason. Ferroelectr. Freq. Control, vol. 41, no. 1, Jan. 1994.

[11] T. Mast, "Empirical relationships between acoustic parameters in human soft tissues", Acoustics Research Letters Online, 1, 37-42 (2000)

[12] A. Selfridge, "Approximate Material Properties in Isotropic Materials," IEEE Trans. Sonics Ultrason., vol. SU-32, no. 3, May 1985.

[13] T. Szabo, *Diagnostic Ultrasound Imaging: Inside Out*, 2nd Ed., Academic Press, 2014.

CONTACT

*J. Kuo, jck226@cornell.edu